Orbifold Tutte Embeddings

Noam Aigerman Yaron Lipman
Weizmann Institute of Science

Abstract

Injective parameterizations of surface meshes are vital for many applications in Computer Graphics, Geometry Processing and related fields. Tutte's embedding, and its generalization to convex combination maps, are among the most popular approaches for computing parameterizations of surface meshes into the plane, as they guarantee injectivity, and their computation only requires solving a sparse linear system. However, they are only applicable to disk-type and toric surface meshes.

In this paper we suggest a generalization of Tutte's embedding to other surface topologies, and in particular the common, yet untreated case, of sphere-type surfaces. The basic idea is to enforce certain boundary conditions on the parameterization so as to achieve a Euclidean orbifold structure. The orbifold-Tutte embedding is a seamless, globally bijective parameterization that, similarly to the classic Tutte embedding, only requires solving a sparse linear system for its computation.

In case the cotangent weights are used, the orbifold-Tutte embedding globally minimizes the Dirichlet energy and is shown to approximate conformal and four-point quasiconformal mappings. As far as we are aware, this is the first fully-linear method that produces bijective approximations to conformal mappings.

Aside from parameterizations, the orbifold-Tutte embedding can be used to generate bijective inter-surface mappings with three or four landmarks and symmetric patterns on sphere-type surfaces.

CR Categories: I.3.5 [Computer Graphics]: Computational Geometry G.1.6 [Numerical Analysis]: Optimization;

Keywords: Tutte embedding, convex combination map, discrete harmonic, conformal maps, injective parameterization

1 Introduction

Mesh parameterization is a central research topic in computer graphics and geometry processing. Only a few algorithms are guaranteed to produce injective parameterizations that are also globally optimal in some well-defined sense. The main approach known to provide such a guarantee is Tutte's embedding [Tutte 1963], and its generalization to convex combination maps (CCM) [Floater 2003a]. One of the attractive properties of CCM is its computational simplicity: it only requires solving a sparse linear system in order to compute the parameterization. However, CCM is currently limited to injective parameterizations of disk-type and toric surfaces, leaving the arguably most common case of spherical surfaces untreated.

Figure 1: *An example of the orbifold-Tutte embedding: a globally bijective mapping of a sphere-type surface (top-left) to a sphere-type Euclidean orbifold (bottom). In the orbifold, boundaries of the same color are topologically identified. Four points on the surface (shown as colored spheres, top-left) are mapped to the four cone singularities of the orbifold (colored disks, bottom). As in this case the orbifold has four cones, each of angle π, and they are placed on the integer grid, the embedding is also a quadrangulation, as shown on the top-right.*

The goal of this paper is to introduce the *orbifold-Tutte* planar embedding, a generalization of Tutte's embedding and CCM to other topologies, and in particular spheres. The orbifold-Tutte embedding bijectively maps the original surface to a canonical, topologically equivalent, two-dimensional flat surface with cone singularities, called a *Euclidean orbifold* (*i.e.*, a pillow-like surface).

The orbifold-Tutte embedding is computed by first cutting the original surface into a topological disk, and second, similarly to CCM, setting the target vertex positions in the plane via two discrete harmonic functions. The new addition is a set of specific boundary conditions that ensure that the target domain is one of the Euclidean orbifolds. The fact that Euclidean orbifolds can be tiled to cover the plane is used to prove the resulting map is a global bijection.

In addition to bijectivity, the orbifold-Tutte embedding has the following desirable properties: 1) It can be interpreted as a seamless homeomorphic mapping of the original surface to one of the Euclidean orbifolds; 2) It is guaranteed to exist and to be computable via a sparse linear system; 3) For symmetric convex combination

weights that approximate the Laplace-Beltrami operator, such as the cotan weights [Pinkall and Polthier 1993], the embedding globally minimizes the Dirichlet energy; For orbifolds with three cones it therefore approximates the conformal mapping, and for orbifolds with four cones it approximates a conformal mapping composed with a global affine transformation. As far as we are aware, this method is the first to provide a bijective approximation to conformal mappings computable via a linear system.

A limitation of our approach is that it is limited to Euclidean orbifolds as target domains, which means that only specific cone singularities can be used; for spheres there are four possible cone structures with 3-4 cones.

Numerical experiments demonstrate that the orbifold-Tutte embedding can be used for efficient computation of bijective, conformal, and seamless parameterizations of large models; see for example Figure 1. Additionally, we show these parameterizations can be used for efficient computation of 4-point bijective quasiconformal mappings between general sphere-type surfaces, and to construct symmetric patterns on surface meshes.

2 Previous work

Tutte's embedding Tutte's embedding [Tutte 1963], later generalized to convex combination maps [Floater 2003a], yields globally injective mappings into the plane by solving a linear system. We briefly review this method at the beginning of Section 3; it is applicable solely for disk-type meshes, and was generalized to the toric case and certain disks with holes in [Gortler et al. 2006]. The toric case is also proved in [Lovász 2004]. Generalizations to the spherical case are usually non-linear [Gotsman et al. 2003] and are not guaranteed to be feasible. Other embeddings of toric and spherical graphs have been discussed in [Castelli Aleardi et al. 2014; Kobourov and Landis 2007].

Conformal parameterizations Approximating conformal parameterizations of surfaces lies in the focus of the parameterization literature (see [Sheffer et al. 2006; Floater and Hormann 2005] for surveys). [Lévy et al. 2002; Desbrun et al. 2002] provide a linear method for approximating conformal parameterizations of disk-type surfaces with free boundaries. [Gu and Yau 2003] generalize to higher genus by considering a pair of discrete harmonic one-forms. These methods, however, are not guaranteed to be injective (globally or per triangle). Non-linear methods are more flexible and use a plethora of representations for conformal maps, *e.g.*, target vertex-positions [Hormann and Greiner 2000], angle space [Sheffer et al. 2005], conformal factors [Springborn et al. 2008; Ben-Chen et al. 2008; Sun et al. 2014], and circle patterns [Kharevych et al. 2006]. [Tsui et al. 2013] compute a parameterization of a sphere-type surface to a hyperbolic orbifold using the method of [Springborn et al. 2008]. [Kazhdan et al. 2012] compute a curvature-flow which converges to a conformal mapping to the sphere. The general shortcoming of non-linear methods is that usually there is no guarantee to obtain a feasible solution, or, if a solution is found, it is not guaranteed to be locally/globally injective, and is not the global minimum of the energy.

Cone manifolds Mapping surfaces to flat cone-manifolds has recently become popular in the context of quadrangulations [Ray et al. 2006; Bommes et al. 2013a]. The mapping is usually computed by one of the following related constructions: flattening the surfaces while relating boundary edges with integer-grid-preserving transformations [Bommes et al. 2013b], integrating two discrete harmonic one forms with a certain singularity structure [Tong et al. 2006], or using a branched covering of the surface [Kälberer et al. 2007]. The emphasis is put on reducing the conformal and isometric distortion [Myles and Zorin 2012; Myles and Zorin 2013]. In this context, two of the four sphere-type Euclidean orbifolds enable quadrangulations of spherical meshes, as shown for example in Figure 1. In general, the Euclidean orbifolds allow 2,3,4, and 6-symmetric parameterizations; that is, bijective parameterizations that conform to symmetric fields of the same order [Palacios and Zhang 2007; Ray et al. 2008; Knöppel et al. 2013].

3 Preliminaries and approach

We denote by $\mathbf{M} = (\mathbf{V}, \mathbf{E}, \mathbf{T})$ an oriented 3-connected disk-type triangular surface-mesh with $n = |\mathbf{V}|$ vertices and a positive weight $w_{ij} > 0$ associated to every half-edge $e_{ij} \in \mathbf{E}$. We denote its boundary vertices by $\partial\mathbf{V}$.

A piecewise-linear function $x : \mathbf{M} \to \mathbb{R}$ is represented by assigning a value per vertex $x_i = x(v_i)$, $v_i \in \mathbf{V}$ encoded in a vector $\mathbf{x} = [x_1, x_2, \ldots, x_n] \in \mathbb{R}^{1\times n}$, and linearly interpolating over each triangle. A *discrete harmonic function* is defined by the following set of linear equations constraining the value at each vertex to be a weighted mean of the values at its neighbours:

$$\sum_{j\in\mathcal{N}_i} w_{ij}\,(x_i - x_j) = 0 \qquad \forall v_i \in \mathbf{V} \tag{1}$$

where $\mathcal{N}_i$ indicates the set of neighbor vertices to $v_i \in \mathbf{V}$.

Discrete harmonic functions are often used to map a disk-type mesh $\mathbf{M}$ to the plane. This is done using two discrete harmonic functions that define a map, $\Phi = (x, y)^T : \mathbf{M} \to \mathbb{R}^2$, represented as the matrix

$$\mathbf{\Phi} = \begin{bmatrix}\mathbf{x}\\ \mathbf{y}\end{bmatrix} \in \mathbb{R}^{2\times n}.$$

Namely, $\mathbf{\Phi}$ is required to satisfy (1) for both $\mathbf{x}$ and $\mathbf{y}$,

$$\sum_{j\in\mathcal{N}_i} w_{ij}\,(\Phi_i - \Phi_j) = 0 \tag{2}$$

where $\Phi_i = [x_i, y_i]^T$ is the i^{th} column of $\mathbf{\Phi}$, and here and after 0 denotes the vector/matrix of zeros in the suitable dimension.

A mapping Φ satisfying (2), *i.e.*, discrete harmonic in each of its coordinates, is called a *convex combination map* (CCM). In case the images Φ_i of boundary vertices $v_i \in \partial\mathbf{V}$ are constrained to vertices of a convex planar polygon, a convex combination map Φ is guaranteed to be a global bijection, as proved by Floater [2003a]. Floater's result is a generalization of the classical result by Tutte [1963] that showed how to realize a planar graph by solving a system of equations similar to (2).

In the case of a toric surface mesh, $\bar{\mathbf{M}}$, Gortler *et al.* [2006] and Lovász [2004] prove that if $\bar{\mathbf{M}}$ is 3-connected then integrating two non-degenerate independent discrete harmonic one-forms of $\bar{\mathbf{M}}$ on a disk-type sub-mesh $\mathbf{M}$ of $\bar{\mathbf{M}}$ also results in a globally bijective mapping, where a discrete harmonic one-form η is an assignment of a value η_{ij} per half-edge that satisfies $\eta_{ij} = -\eta_{ji}$ and is closed and co-closed. This flattening utilizes the fact that the plane is the universal cover of the torus [Gu and Yau 2003].

This does not address the spherical case: in contrast to a disk, a sphere is not homeomorphic to any subset of the plane , and hence cannot be mapped without introducing discontinuities to the map, and unlike the torus its universal cover is the sphere again - so how can one construct a Tutte-type embedding in this case? As it turns out, adding cone singularities allows mapping the sphere to a sphere-type flat surface called a *Euclidean orbifold*, denoted $\mathcal{O}$. The special symmetry properties of the Euclidean orbifolds yield a simple construction of globally bijective discrete harmonic embeddings of the sphere.

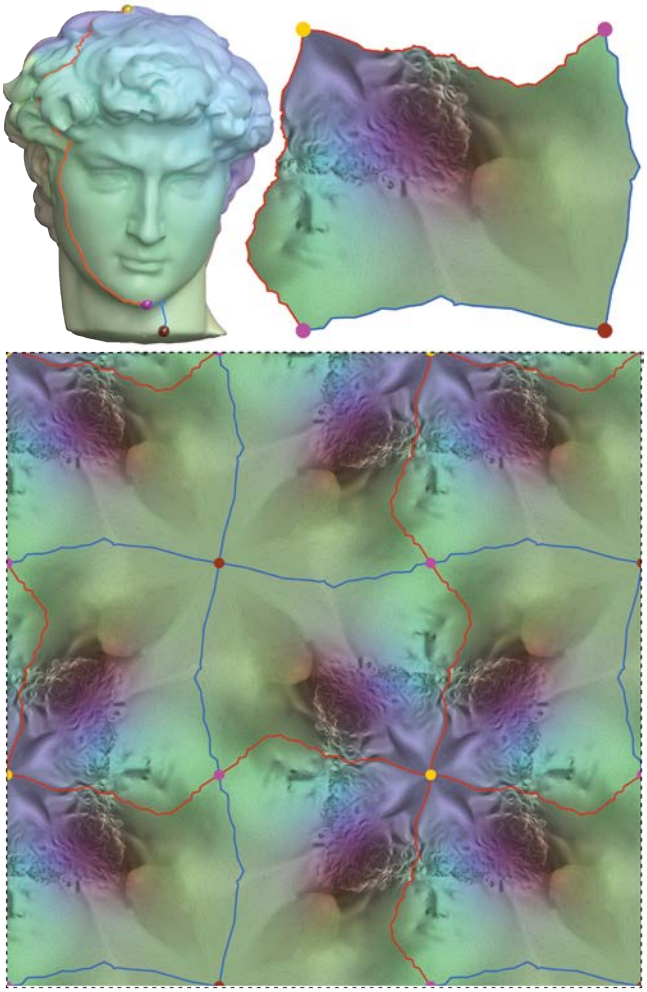

Figure 2: *The orbifold-Tutte framework: David's bust is cut open through the three cone singularities and embedded to a tile in the plane. This tile represents a sphere-type Euclidean orbifold structure, upon identifying the two sides of the cuts (colored with the same color). The orbifold symmetry enables gluing copies of the tile to cover the plane: this is the property that ensures the map is globally bijective.*

Before providing an exact definition of a Euclidean orbifold, let us start with a motivating example: Figure 2 shows a tiling of the plane (bottom) using a basic tile (top-right). This tile is the injective parameterization of David's head computed by our method, after cutting the mesh into a disk (cuts visualized as colored curves, top-left). Although the tile is a disk, once its boundaries are identified according to the original topology of the uncut mesh (*i.e.*, boundaries with the same color are "glued back together") it also defines a topological sphere. This topological sphere is an example of a Euclidean orbifold: It is *flat* everywhere, that is, each vertex has an angle sum of 2π, except for a few special vertices (marked as colored points) where there are cone singularities. At a cone singularity the total angle sum differs from 2π; for example, at the yellow cone-singularity the angle-sum is $\pi/2$, *i.e.*, its 1-ring is mapped to only a quarter of a circle. Note that the purple cone singularity appears twice in the orbifold's tile with a total angle sum of π, and that every boundary vertex which is not a cone is regular and has an angle sum of 2π in the "uncut" topology. Therefore in this example there are exactly three cone singularities with angles $\pi/2, \pi, \pi/2$.

The resulting embedding has three key properties:

1. **Boundaryless:** The cuts on David's head are used for the computation of the map, however the final map is indifferent to their particular choice.

2. **Harmonicity:** This mapping is discrete-harmonic at all vertices except at the cone vertices. That is, each vertex is at the weighted mean of its neighbours on the glued mesh (the tiling).

3. **Global injectivity:** The special symmetry properties of the Euclidean orbifold, which ensure that the tile representing the orbifold can be used to tile the plane, will be the key for proving that this parameterization is globally injective.

4 Method

The orbifold-Tutte embedding $\bar{\Phi} : \bar{\mathbf{M}} \to \mathcal{O}$ will be realized by three steps:

1. Deciding on the placement of the cone singularities at vertices of $\bar{\mathbf{M}}$ according to user-input.

2. Cutting $\bar{\mathbf{M}}$ through the cone vertices to achieve a disk-type surface $\mathbf{M}$ (as in Figure 2, top-left).

3. Solving a sparse linear problem to obtain the discrete harmonic parameterization $\Phi : \mathbf{M} \to \mathbb{R}^2$ of $\mathbf{M}$ to a planar orbifold tile that realizes the conceptual mapping of the uncut mesh to the orbifold $\bar{\Phi} : \bar{\mathbf{M}} \to \mathcal{O}$.

The main focus is on Step 3. The idea is to define Φ by solving the regular CCM equations (2) but to modify them at the boundary vertices so as to account for the orbifold structure: first, we map the cone vertices to certain fixed locations in the plane. Second, we require that the two "sides" of each cut are rotated copies of one-another, where the rotation angle is decided according to the cone singularities (*e.g.*, at Figure 2, the two sides of the red cut are identical up to a $\pi/2$ rotation). This ensures the resulting embedding is indeed tileable. Third, we require that each boundary vertex that is not a cone also satisfies the convex combination property once the mesh is glued back together, *i.e.*, in the tiling.

We begin by exploring the different sphere-type Euclidean orbifolds and their cone singularity structure. We then move to providing the full details to Steps 2 and 3.

Euclidean orbifolds and cone singularities Euclidean orbifolds are two dimensional flat surfaces (*i.e.*, with zero curvature everywhere) with cone singularities. The Euclidean orbifolds are in one-to-one correspondence with the 17 *wallpaper groups* [Conway et al. 2008]. A wallpaper group is a group of isometries of the Euclidean plane (translations, rotations, reflections, and their compositions) that contains two translations in independent directions $\tau_1, \tau_2 \in \mathbb{R}^2$.

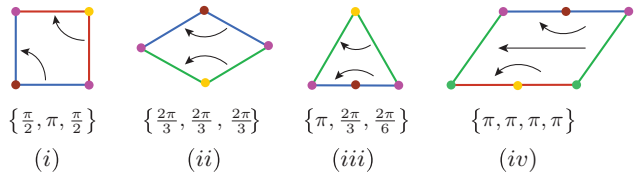

Figure 3: *The basic tiles (top) and cone angles of the four different sphere-type Euclidean orbifolds.*

Euclidean orbifolds are defined to be the quotient of the plane $\mathbb{R}^2$ by the corresponding wallpaper group. That is, the orbifold $\mathcal{O} = \mathcal{O}_G = \mathbb{R}^2/G$, corresponding to a wallpaper group G, has one point per orbit of G, where an orbit of a point $p \in \mathbb{R}^2$ is an equivalence class defined by $[p] = \{g(p) | g \in G\}$. A Euclidean orbifold can be used to tile the plane (using actions from the group G) after it is cut through its cones to a topological disk. We refer to such a disk as a *tile* of the orbifold. Note that the tile of an orbifold is not unique, as a tile can be seen as a choice of a representative member from each orbit, *i.e.*, $p^* \in [p]$.

We focus mainly on sphere-type orbifolds (although we will demonstrate embeddings to topologically different Euclidean orbifolds as well in Section 6). There are in total four types of sphere-type Euclidean orbifolds that are created from four different wallpaper groups and differ in their number of cones and their angles. For example, Figure 2 maps David's head to an orbifold with cone angles $\{\pi/2, \pi, \pi/2\}$ which can be imagined as a triangular pillow.

An instructive way to enumerate the possible cone singularities of sphere-type Euclidean orbifolds is to consider the angle deficit at the cones

$$\delta_j = 2\pi - \Theta_j \tag{3}$$

where Θ_j is the cone angle of the j^{th} cone singularity. Since a tile of the orbifold can be used to tile the plane, a necessary condition is that the cone angles will each satisfy

$$\Theta_j = \frac{2\pi}{k_j} \tag{4}$$

where $k_j \geq 2$ is a positive integer. Considering the Gauss-Bonnet theorem for cone manifolds [Schwartz 2011] we get that

$$\sum_j \delta_j = 2\pi\chi(\mathcal{O}) = 4\pi \tag{5}$$

where we used the fact that the Euler Characteristic of a sphere is 2. All possible cone angles $\{\Theta_1, \Theta_2, \dots\}$ that satisfy (4) and (5) indeed exhaust the cone structures of all Euclidean sphere-type orbifolds. We identify each sphere-type orbifold via its cone singularity structure (number of cones and their angles) and represent the orbifold using one of its tiles in the plane, namely the one in which the cone-singularity points are connected by straight lines. We name this particular choice of tile the *basic tile*. This is summarized in Figure 3. Note that the cone singularities dictate the angles of the basic tile. Each of the basic tiles defines the target domain of the parameterization to be constructed $\Phi : \mathbf{M} \to \mathbb{R}^2$.

We shall denote by $\bar{\mathcal{C}} = \{\bar{v}_1, \bar{v}_2, .., \bar{v}_I\} \subset \bar{\mathbf{V}}$, $I \in \{3, 4\}$ the set of three or four vertices of the mesh $\bar{\mathbf{M}}$ that will be mapped to the cones of the chosen target Euclidean orbifold in Figure 3.

Cutting to disk topology In the next step we cut the sphere-type input mesh $\bar{\mathbf{M}}$ to a disk $\mathbf{M}$ by cutting along edges between the cone singularity vertices $\bar{v}_1 \to \bar{v}_2 \to \cdots \to \bar{v}_I$. As we later show, the particular choice of this cut has no affect on $\bar{\Phi}$ for types (i), (ii), (iii). For type (iv) any choice of homotopic cuts will result in the same $\bar{\Phi}$. That is, the output of the algorithm only depends on the choice of cone singularities. However, note that differently from the orbifold mapping $\bar{\Phi}$, the mapping of the cut mesh to the plane Φ does change according to the cut. We denote by $\mathcal{C} = \{v_1, v_2, .., v_J\} \subset \mathbf{V}$, $J \in \{4, 6\}$ the duplicated cone singularities in the cut mesh $\mathbf{M}$.

Formulating the linear system We construct a sparse square linear system

$$A \operatorname{vec}(\mathbf{\Phi}) = b \tag{6}$$

with $A \in \mathbb{R}^{2n \times 2n}$, $b \in \mathbb{R}^{2n \times 1}$, and $\operatorname{vec}(\mathbf{\Phi}) \in \mathbb{R}^{2n \times 1}$ is the column stack vector of the unknown matrix $\mathbf{\Phi} \in \mathbb{R}^{2 \times n}$ defining the orbifold-Tutte parameterization $\Phi : \mathbf{M} \to \mathbb{R}^2$. The linear system (6) is constructed by putting together three sets of linear equations as follows.

First, for all interior vertices $v_i \in \mathbf{V} \setminus \partial\mathbf{V}$ we set the standard discrete harmonic equation as in (2),

$$\sum_{j \in \mathcal{N}_i} w_{ij} \left(\Phi_i - \Phi_j\right) = 0. \tag{7}$$

The second set of equations deals with the cone-singularity vertices $v_k \in \mathcal{C}$. Let $\Phi_1^{\mathcal{C}}, \Phi_2^{\mathcal{C}}, \dots, \Phi_J^{\mathcal{C}}$ be the cone positions of the orbifold basic tile as shown in Figure 3 (visualized as colored dots). We set the following positional constraints

$$\Phi_k = \Phi_k^{\mathcal{C}}, \tag{8}$$

for $k = 1, .., J$. Note that for orbifolds of type $(i), (ii), (iii)$ the target cone positions $\Phi_k^{\mathcal{C}}$ can be chosen up to an arbitrary global similarity transformation, while for type (iv) they can be chosen up to a non-degenerate affine transformation, that is, any parallelogram can be chosen as the basic tile of the type (iv) orbifold instead of the one picked in Figure 3.

In the last set of equations we deal with boundary vertices that are not cones $v_i \in \partial\mathbf{V} \setminus \mathcal{C}$. Each such vertex has a *twin* vertex $v_{i'}$ in the other copy of the cut (*i.e.*, $v_i, v_{i'}$ correspond to the same vertex in the uncut mesh $\bar{\mathbf{M}}$), and a rotation $R_{i'i}$ relating them (according to the cone singularity), as shown in the inset for a type (i) orbifold. For each such pair $v_i, v_{i'}$ we set the following two equations

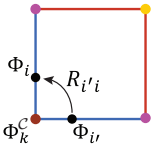

$$\sum_{j \in \mathcal{N}_i} w_{ij} \left(\Phi_i - \Phi_j\right) + \sum_{j \in \mathcal{N}_{i'}} w_{i'j} \, R_{i'i} (\Phi_{i'} - \Phi_j) = 0 \tag{9a}$$

$$R_{i'i} \left(\Phi_{i'} - \Phi_k^{\mathcal{C}}\right) - \left(\Phi_i - \Phi_k^{\mathcal{C}}\right) = 0 \tag{9b}$$

where v_k is the joint cone vertex of $v_i, v_{i'}$, see inset again for an illustration. Intuitively, the first equation ensures that Φ will have the convex combination property across the boundary, that is, the "glued" tiling is discrete harmonic also at vertices on the cut. The second equation makes sure that both copies of each cut are identical up to a rotation.

Combining equations (7),(8),(9) we construct A, b in (6). Solving (6) for $\mathbf{\Phi}$ defines the piecewise-linear parameterization $\Phi = (x, y)^T : \mathbf{M} \to \mathbb{R}^2$ mapping $\mathbf{M}$ to an orbifold tile in the plane.

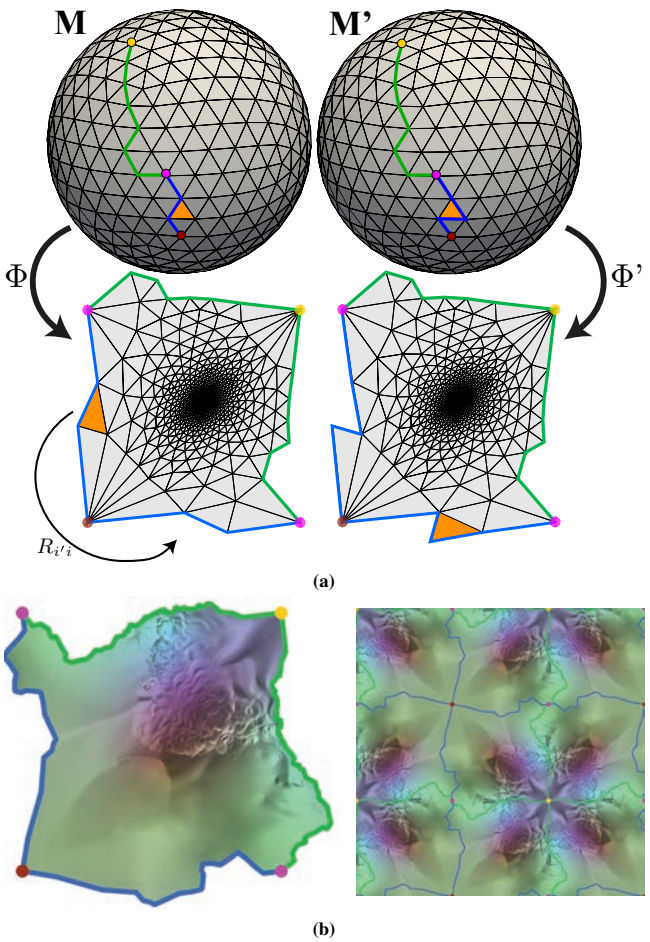

Figure 4: *The seamlessness of the embedding: (a) two embeddings computed for different cuts are identical up to a transformation $R_{i'i}$ of triangles across the cut. (b) modifying the cuts in Figure 2 yields a different parameterization Φ, however it yields the exact same tiling and as a result the exact same orbifold embedding $\bar{\Phi}$.*

5 Properties

We prove correctness of the algorithm presented in Section 4, namely proving that $\Phi : \mathbf{M} \to \mathbb{R}^2$ is globally injective and that it induces a boundaryless homeomorphism $\bar{\Phi} : \bar{\mathbf{M}} \to \mathcal{O}$. We further discuss how the orbifold-Tutte embedding can be used for approximating conformal maps.

Definition of $\bar{\Phi}$ and its boundaryless property Let us first define $\bar{\Phi} : \bar{\mathbf{M}} \to \mathcal{O}$ given $\Phi : \mathbf{M} \to \mathbb{R}^2$. The orbifold $\mathcal{O}$ is constructed from orbits $[p]$, $p \in \mathbb{R}^2$; that is, every point in $\mathcal{O}$ is identified with an orbit of the group G. Denote by $\mathfrak{o} : \mathbb{R}^2 \to \mathcal{O}$ the map defined by $\mathfrak{o}(p) = [p]$. Let $\bar{p} \in \bar{\mathbf{M}}$ be a point on the uncut mesh, let $p \in \mathbf{M}$ be a point on the cut mesh which is one of the copies of $\bar{p}$ after the cutting of the mesh has been performed (if $\bar{p}$ is away from the cut then there is only one copy p; if it is on the cut then it is duplicated into two copies). Now, define the mapping of the uncut mesh to the orbifold as $\bar{\Phi}(\bar{p}) \triangleq \mathfrak{o}(\Phi(p))$. To see that $\bar{\Phi}$ is well defined for points on the cut which are duplicated in the cutting process, note that any other copy $p' \in \mathbf{M}$ of $\bar{p}$ will produce $\Phi(p')$ in the same orbit of $\Phi(p)$ due to (9b).

To explain the boundaryless property, we use the notion of cut homotopy (see [Aigerman et al. 2015]), defined by changing the cut one triangle at a time and without causing self-intersections. We claim that two homotopic cuts will always produce the same orbifold embedding map $\bar{\Phi} : \bar{\mathbf{M}} \to \mathcal{O}$. Indeed, consider a solution $\mathbf{\Phi}$ to (6) as shown in Figure 4a, left, and consider the orange triangle lying on the boundary. Moving this boundary triangle using the relevant transformation $R_{i'i}$ will create a new solution of (6), $\mathbf{\Phi}'$ (Figure 4a, right) for a new cut-mesh, $\mathbf{M}'$, which is $\bar{\mathbf{M}}$ cut to a disk with a different, homotopic cut.

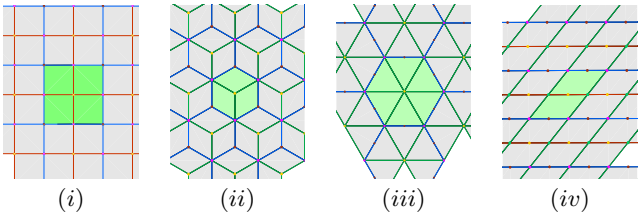

Figure 5: *Tiling the plane with the basic orbifold tiles from Figure 3. In light green we show the torus covered with the basic tiles.*

As we show in the next subsection, Eq. (6) is non-singular and therefore $\mathbf{\Phi}'$ is the unique solution to it, entailing that had we chosen a different cut resulting in $\mathbf{M}'$ and then solved (6), we would have gotten exactly $\mathbf{\Phi}'$. This procedure of homotopically moving triangles can be repeated to build a solution $\mathbf{\Phi}''$ of (6) to any homotopic cut of $\bar{\mathbf{M}}$. Since we modified the embedding using transformations from the group G, for every $\bar{p} \in \bar{\mathbf{M}}$ and its copy $p \in \mathbf{M}$, we have that $\Phi''(p)$ will differ from $\Phi(p)$ by an element of the group G. Therefore, $\Phi''(p)$ and $\Phi(p)$ will both reside in the same orbit of G and $\mathfrak{o}(\Phi''(p)) = \mathfrak{o}(\Phi(p))$. This implies that $\bar{\Phi}'' = \bar{\Phi}$. Indeed, in Figure 4b we have arbitrarily modified the cuts on David's head, shown in Figure 2, and recomputed the embedding. Although the embedding Φ is different, it still induces the same tiling as in Figure 2 and as a result the same orbifold embedding $\bar{\Phi}$.

For three cones on the sphere all cuts are homotopic so in this case the result is independent of the cut choice. For four cones, there exist non-homotopic cuts and therefore the algorithm will produce the same orbifold embedding only for cuts that are homotopic.

Globally injective mapping We prove that the linear system (6) has a unique solution and that this solution leads to a globally injective mappings $\Phi : \mathbf{M} \to \mathbb{R}^2$ and consequently a homeomorphism $\bar{\Phi} : \bar{\mathbf{M}} \to \mathcal{O}$. We first show that the constructed linear system has a unique solution, by showing its matrix is non-singular:

Theorem 1. *The matrix A in* (6) *is non-singular.*

The proof of the theorem is technical and is given in Appendix A. We now consider the unique solution $\mathbf{\Phi}$ to Eq. (6), and prove that $\Phi : \mathbf{M} \to \mathbb{R}^2$ is injective.

Theorem 2. *A discrete harmonic mapping $\Phi : \boldsymbol{M} \to \mathbb{R}^2$ of a 3-connected disk-type mesh $\boldsymbol{M}$ satisfying the sparse linear system* (6) *is globally injective.*

Proof. Equations (8), (9b) imply that the cones of $\mathbf{M}$ are mapped to the cone points of a basic tile (see Figure 3 for sphere-type basic tiles) and images of twin boundary vertices in $\mathbf{M}$ (*i.e.*, boundaries that originated from a single cut in $\bar{\mathbf{M}}$) are related by rotations which are fixed according to the cone angles (the rotations are shown using black arrows in the basic tiles in Figure 3).

For any element $g \in G$, we denote by $\Phi^g = g \circ \Phi$ the composition of Φ with the transformation g. We also make a copy $\mathbf{M}^g$ of $\mathbf{M}$ for every $g \in G$. We say two copies $\mathbf{M}^g, \mathbf{M}^h$ are *neighbors* if the basic tiles corresponding to $\Phi^g(\mathbf{M}^g)$, $\Phi^h(\mathbf{M}^h)$ share an edge; Figure 5 shows the tiling of the plane using the basic tiles from Figure 3. If $\mathbf{M}^g, \mathbf{M}^h$ are neighbors they share a boundary segment corresponding to that basic edge.

Every wallpaper group G is a *semi-direct product* $G = T \rtimes O$ of a translation group $T = \langle \tau_1, \tau_2 \rangle$, generated by two independent translations $\tau_1, \tau_2 \in \mathbb{R}^2$, and a point group O (discrete subgroup of the orthogonal transformation group). A semi-direct product means that every transformation $g \in G$ can be written uniquely as $t \circ R$, where $t \in T$ a translation and $R \in O$ an orthogonal transformation.

Consider all copies $\mathbf{M}^{g_j}$ corresponding to elements of the point group, $g_j \in O$ and stitch neighboring copies along common boundary edges. Denote the resulting disk-type surface $\boldsymbol{\mathcal{M}}$. We define the map $\Phi_{\boldsymbol{\mathcal{M}}} : \boldsymbol{\mathcal{M}} \to \mathbb{R}^2$ by mapping each vertex $v_i \in \mathbf{M}^{g_j} \subset \boldsymbol{\mathcal{M}}$ according to $\Phi^{g_j}(v_i)$. Now, by the decomposition $G = T \rtimes O$ we know that the boundary edges of $\Phi_{\boldsymbol{\mathcal{M}}}(\boldsymbol{\mathcal{M}})$ can be identified using only translations from T. This allows to consider $\boldsymbol{\mathcal{M}}$ to be a disk submesh of a torus (as shown in the inset), and $\Phi_{\boldsymbol{\mathcal{M}}}$ a piecewise linear parameterization of it to the plane. Figure 5 shows in light green examples of the planar image of this disk submesh of a torus, *i.e.*, $\Phi_{\boldsymbol{\mathcal{M}}}(\boldsymbol{\mathcal{M}})$, for the basic orbifold tiles of Figure 3.

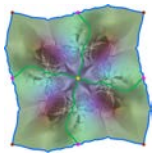

So far we have a mapping $\Phi_{\boldsymbol{\mathcal{M}}}$ of a disk submesh of a torus to the plane. To finish the proof we need to show $\Phi_{\boldsymbol{\mathcal{M}}}$ is a non-degenerate (*i.e.*, its image is not a point or contained in a line) convex combination map. The non-degeneracy is clear from the boundary conditions (8). Eq. (7) ensures that each map $\Phi^{g_j} : \mathbf{M}^{g_j} \subset \boldsymbol{\mathcal{M}} \to \mathbb{R}^2$ satisfies the convex combination property at all interior vertices of $\mathbf{M}^{g_j}$. Eq. (9a) ensures that the map $\Phi_{\boldsymbol{\mathcal{M}}}$ satisfies the convex combination property at stitched boundaries of neighboring copies $\mathbf{M}^{g_j}, \mathbf{M}^{g_k}$ and across identified boundaries of the torus. Lastly, $\Phi_{\boldsymbol{\mathcal{M}}}$ also satisfies the convex combination property at the center cone in $\boldsymbol{\mathcal{M}}$ (*e.g.*, the center yellow point in Figure 5 and the inset above) since at the cone we have the 1-ring neighborhood of the relevant cone vertex in $\mathbf{M}$ duplicated and rotated by elements of a point group. For example, in case of the type (i) orbifold, the point group contains rotations by $0, \pi/2, \pi, 3\pi/2$. $\Phi_{\boldsymbol{\mathcal{M}}}$ therefore defines two non-degenerate, independent discrete harmonic one-forms on a torus, and in view of the above mentioned result by Gortler *et al.*, [2006], $\Phi_{\boldsymbol{\mathcal{M}}}$ is globally injective, and therefore $\Phi(\mathbf{M}) = \Phi^e(\mathbf{M}^e)$, where e is the identity transformation, is globally injective as well. This concludes the proof. □

The injectivity of Φ, proven in Theorem 2, implies that Φ maps $\mathbf{M}$ bijectively to some tile of the respective orbifold. Therefore, the mapping $\bar{\Phi} = \mathfrak{o} \circ \Phi$ to the orbifold $\mathcal{O}$ is bijective. We summarize:

Theorem 3. *Let $\bar{\boldsymbol{M}}$ be a sphere-type mesh with a prescribed set of three or four distinct vertices $\bar{\mathcal{C}} \subset \bar{\boldsymbol{V}}$. Let $\boldsymbol{M}$ be a 3-connected disk-type submesh of $\bar{\boldsymbol{M}}$ with the vertices $\bar{\mathcal{C}}$ at its boundary. A discrete harmonic mapping $\Phi : \boldsymbol{M} \to \mathbb{R}^2$ of $\boldsymbol{M}$ satisfying the sparse linear system* (6) *defines a homeomorphism $\bar{\Phi} : \bar{\boldsymbol{M}} \to \mathcal{O}$, where $\mathcal{O}$ is a sphere-type Euclidean orbifold.*

We note that the above theorems are actually applicable to general Euclidean orbifolds, not just sphere-type, and therefore can be used to map other topologies than spheres. We discuss this shortly in Section 6. Furthermore, note that taking the translational wallpaper group T generates the toric embedding from Gortler *et al.*, [2006] and Lovasz [2004]; in that sense the orbifold-Tutte is a generalization of the previous toric embeddings.

Approximating conformal mappings When the weights w_{ij} are symmetric, *i.e.*, $w_{ij} = w_{ji}$, the mapping Φ can be given a variational interpretation as a global minimizer of the convex quadratic energy

$$E(\boldsymbol{\Phi}) = \frac{1}{2} \sum_{e_{ij} \in \mathbf{E}} w_{ij} \left\| \Phi_i - \Phi_j \right\|^2, \tag{10}$$

under the linear constraints (8), (9b).

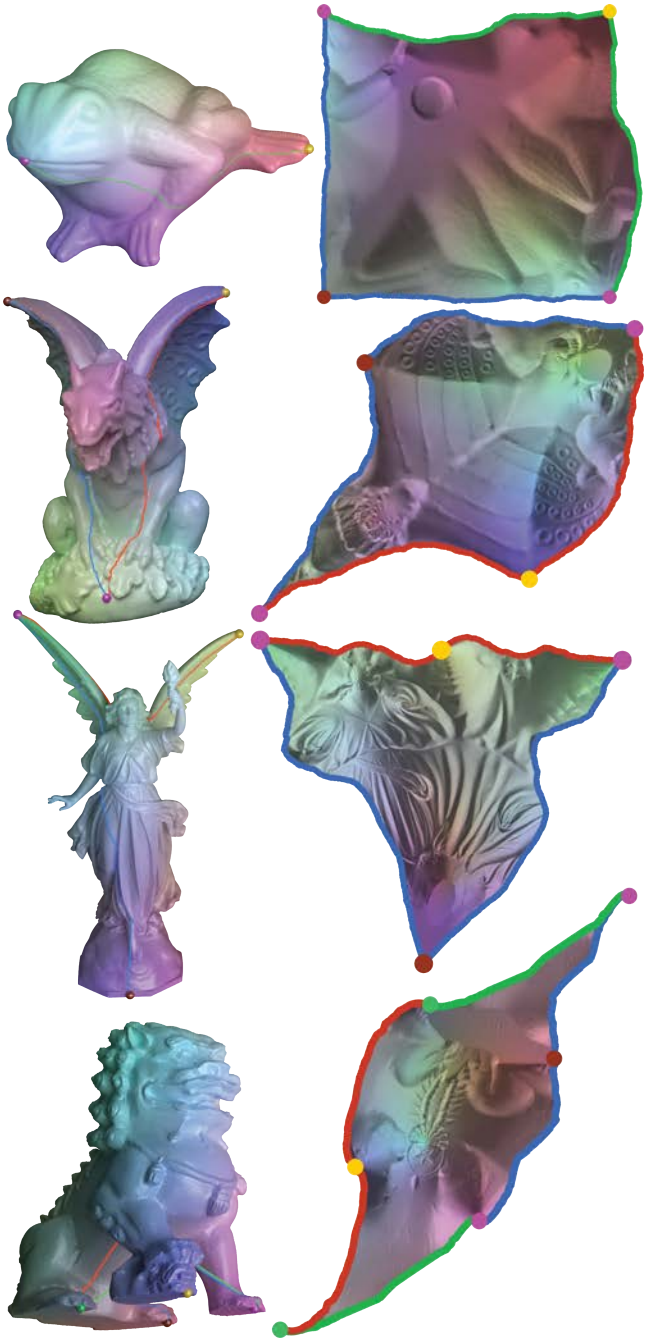

Figure 6: *Embeddings of the 4 orbifold types, with MVC weights.*

An archetypal example (assuming the mesh $\mathbf{M}$ is intrinsic-Delaunay) is to take $w_{ij} > 0$ to be the well-known cotan weights [Pinkall and Polthier 1993]. In this case, the above energy is the Dirichlet energy of the piecewise linear mapping Φ,

$$E_D(\boldsymbol{\Phi}) = \frac{1}{2} \int_{\mathbf{M}} |\nabla \Phi|^2 . \tag{11}$$

It can be shown that minimizing (10) with the linear boundary constraints (8),(9b) is equivalent to solving the linear system (6). Since all the injective piecewise linear maps Φ' that satisfy the boundary constraints (8),(9b) have the same target area, $\mathrm{Area}(\Phi(\mathbf{M}))$, that is the area of the basic orbifold tile, the map Φ can be seen as the one

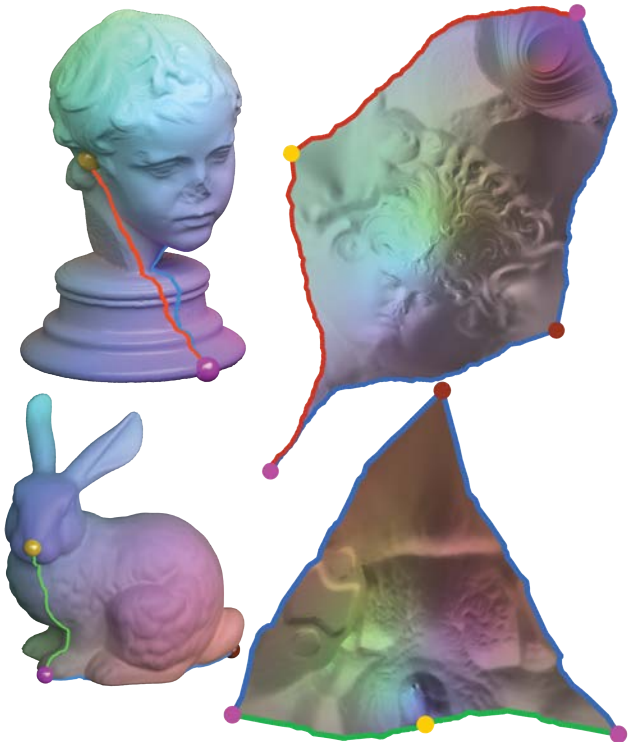

Figure 7: *Harmonic parameterizations of type (ii) and (iii) orbifolds using cotangent weights.*

globally minimizing the conformal energy

$$E_C(\mathbf{\Phi}) = E_D(\mathbf{\Phi}) - \text{Area}(\mathbf{\Phi}) \tag{12}$$

among bijective maps from $\bar{\mathbf{M}}$ to the orbifold $\mathcal{O}$. For orbifolds of types $(i), (ii), (iii)$ (that have precisely three cones) this means that Φ is approximating the unique conformal map taking v_1, v_2, v_3 to the cones of the respective orbifold. For the type (iv) orbifold we get an approximation of a conformal map composed with a global affine transformation. We show empirical results validating these claims in Section 6.

6 Results

We now show results obtained by our method. We discuss mesh parameterizations and show applications to inter-surface mappings, symmetric fields on meshes, and extensions to other Euclidean orbifolds.

6.1 Parameterizations

We have experimented with the orbifold-Tutte embedding for computing seamless bijective parameterizations $\bar{\Phi} : \bar{\mathbf{M}} \to \mathcal{O}$, with two choices of weights w_{ij}: mean value coordinates [Floater 2003b], and cotangent weights [Pinkall and Polthier 1993].

Mean Value coordinates Figure 6 shows embeddings of four sphere-type meshes to the four possible orbifold types (i)-(iv) using mean value coordinates (MVC). Since MVC is guaranteed to generate positive edge weights, Theorem 2 guarantees all these parameterizations are injective. Note that the boundary of the target image is non-convex.

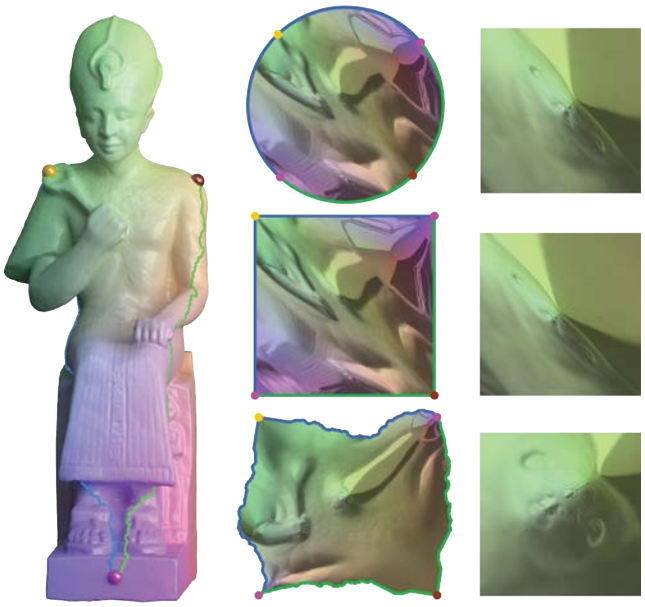

Figure 8: *Comparison of our method (bottom), to the classic Tutte embedding onto a convex domain with fixed boundary (top and middle). Our method does not introduce strong angle distortion, as opposed to the classic use of CCM.*

Cotangent weights Figure 7 shows two orbifold-Tutte parameterizations using the cotan weights to type (ii) and (iii) orbifolds. As these orbifolds have exactly three cones the parameterization is approximately conformal, as we have explained in Section 5.

Figure 8 compares two discrete harmonic mappings with fixed, arc-length boundary conditions (top two rows) with our "boundaryless" orbifold boundary conditions (bottom row). Fixing the boundary greatly affects the parameterization and results in noticeable distortion, *e.g.*, at the head of the statue, as shown in the blowups. In the orbifold embedding, the target domain can also be thought of as a square, but since the image of the cuts is not explicitly constrained, the distortion can be further reduced without any noticeable artifacts at the boundary.

Conformal maps As explained in Section 5 using cotan weights leads to approximations of conformal maps, as shown in the inset. In Figure 9 we depict the conformal distortion (blue for low, red for high) of two orbifold parameterizations using cotan weights. The conformal distortion histograms show average conformal distortion below 1.05 that implies a very good approximation of true angle-preserving maps. Note that the Bimba model is mapped to a type (i) orbifold which has two cones with angles $\pi/2$ and a third cone with angle π. As expected, in the vicinity of the $\pi/2$ cones the conformal distortion is higher, and will get concentrated more locally at the cones as the mesh is refined. Indeed, Figure 10 depicts exactly this phenomenon: upon refinement, the distortion becomes concentrated around the cones. Furthermore, as the histograms show, the overall conformal distortion decreases, as excepted, toward the smooth conformal map with perfect conformal distortion of 1 everywhere except at cone singularities.

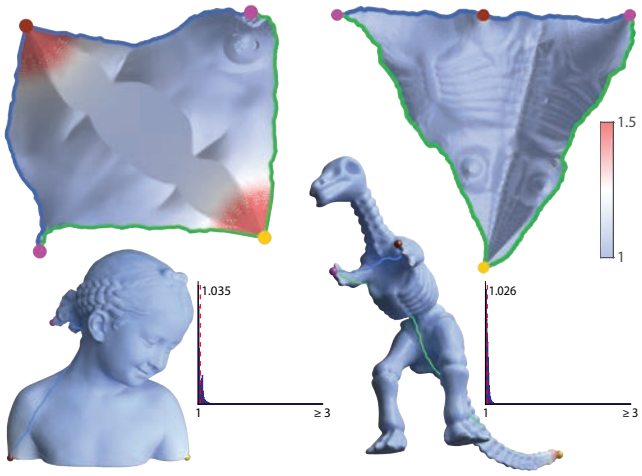

Figure 9: *Embeddings of type (i) and (iii), colored according to conformal distortion and with distortion histograms.*

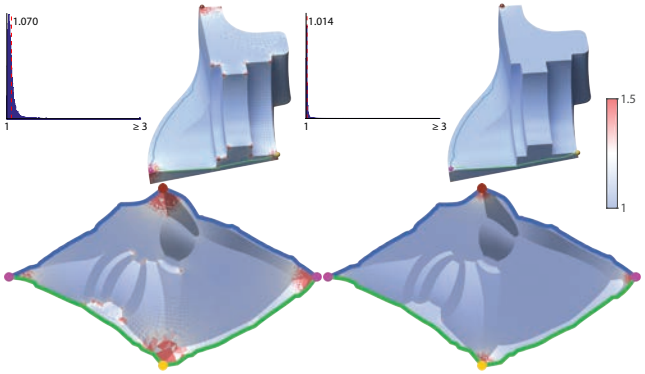

Figure 10: *Two embeddings of the same surface with the same prescribed singularities. Once of the original mesh (left) and once of a refined version (right). The embedding converges to a conformal map.*

Setting the affine degree of freedom for the type (iv) orbifold The tiles of orbifolds of type (i), (ii), (iii) are defined up to a global similarity that does not change conformal distortion. Orbifolds of type (iv) have four cone points and are defined up to a non-degenerate affine transformation. When solving (6) we pick one arbitrary instance fixed by our basic type (iv) tile (see Figure 3). Indeed, let $\mathbf{\Phi}$ be a solution to (6) with type (iv) boundary conditions, and let $L \in \mathbb{R}^{2\times 2}$ denote an arbitrary linear transformation of $\mathbb{R}^2$. Then, it can be verified that $\mathbf{\Phi}' \equiv L\mathbf{\Phi}$ is a solution to (6) when Φ_k^C are replaced with $L\Phi_k^C$ in Equations (8) and (9b). This is due to the fact that rotations by $0, \pi$ (the only ones present in the type (iv) orbifold) commute with L; therefore, L preserves both the boundary conditions of the basic tile as well as the discrete harmonicity of the tiling.

It is however rather simple to set this degree of freedom so as to minimize the conformal distortion of the embedding. As advocated in Section 5 we will choose the linear transformation that minimizes the conformal distortion (12), also known as the least-squares conformal energy [Lévy et al. 2002]. Since E_C is not scale invariant (in fact, it can be seen as the square deviation of Φ from satisfying the Cauchy-Riemann equations) we cannot minimize E_C over all linear L as that would lead to the zero solution.

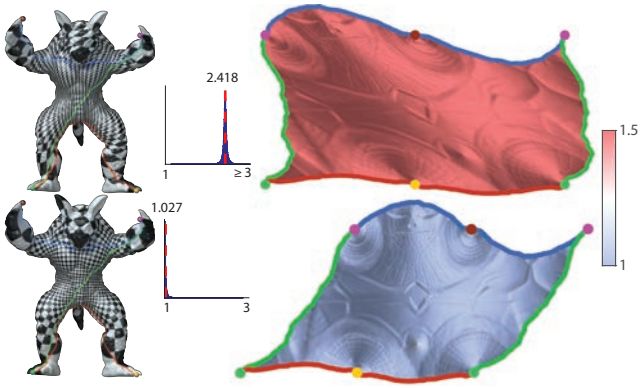

Figure 11: *A type (iv) embedding, before and after computing the global affine transformation to minimize the conformal energy of the embedding.*

Instead, we minimize it over the unit sphere:

$$\min_{L} \quad E_C\left(L\mathbf{\Phi}\right) \tag{13a}$$

$$\text{s.t.} \quad \|L\|_F^2 = 1 \tag{13b}$$

This optimization problem is solved by taking the eigenvector of the 4×4 Hessian of the quadratic form $E_C(L\mathbf{\Phi})$ (as a function of the entries of L) corresponding to the minimal eigenvalue.

Figure 11 shows two type (iv) orbifold embeddings: Top row, the original, "arbitrary" Φ; and bottom row, after choosing the affine degree of freedom according to (13). After applying this affine map the conformal distortion histogram has shifted toward zero and produced average conformal distortion below 1.03. This result is consistent with all examples we have tried. Throughout the paper, we use this method when computing a type (iv) orbifold embedding.

Comparison to CETM Figure 12 shows a comparison with Conformal Equivalence of Triangle Meshes [Springborn et al. 2008], where we reproduce an example from that paper: the Venus model is mapped to a conformally-equivalent triangle mesh with a flat metric and four cones of angle π. We reproduce this example by using the orbifold-Tutte embedding to a type (iv) orbifold, which has this exact cone structure. Noticeably, the two parameterizations are very similar. One difference is that the CETM produces a slightly lower average conformal distortion while the orbifold-Tutte embedding provides a lower maximal conformal-distortion (2.7, compared to CETM's maximal distoriton of 9.1). CETM minimizes a convex energy over a non-convex domain and is not guaranteed to produce a valid metric/parameterization. This is in contrast to the linear orbifold-Tutte embedding that guarantees a bijective solution. A drawback of the orbifold-Tutte method in comparison to CETM, however, is that it can only handle a particular cone structure.

Symmetric patterns The orbifold-Tutte embedding enables generating symmetric patterns on the original surface mesh: Since the orbifold is defined as the quotient of the plane by a wallpaper group, if one chooses a symmetric pattern which is invariant to the wallpaper group's transformations, then pulling the pattern back results in a seamless symmetric pattern on the surface (*e.g.*, in Figure 1 we show quads). In Figure 14 we show texturing with stripes (2-field) using the type (iv) orbifold, and equilateral triangles (3-field) using the type (ii) orbifold.

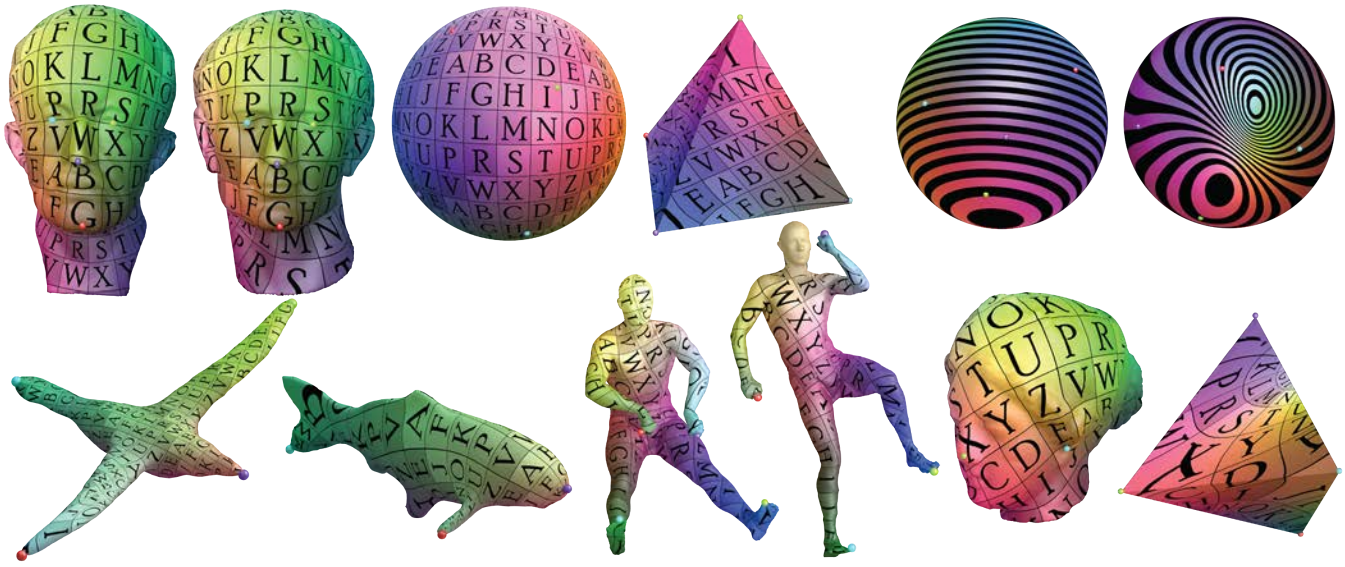

Figure 13: *By embedding two meshes into the same orbifold, we can compute seamless bijective maps between a pair of surfaces, interpolating the given 3 or 4 landmark constraints.*

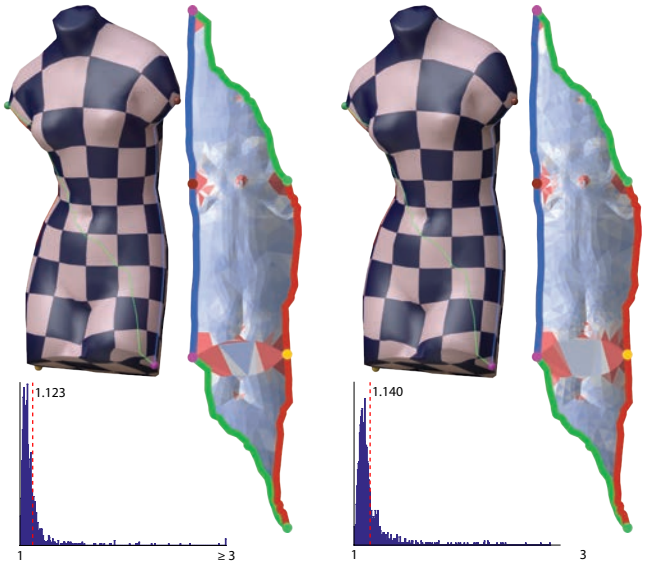

Figure 12: *Comparison of CETM [Springborn et al. 2008] (left) to our method (right) in terms of conformality. The two embeddings are very similar and yield similar distortion profiles, however ours is obtained by merely solving a sparse linear system.*

6.2 Surface-to-surface homeomorphisms

A useful application of the orbifold-Tutte embedding is computing inter-surface maps that are continuous, bijective, seamless, and interpolate a set of three or four landmark positions. For three landmarks the surface-map approximates the smooth conformal map interpolating the landmarks, and for four points, the interpolating extremal quasiconformal map.

The map $f : \mathbf{M}_1 \to \mathbf{M}_2$ is constructed by mapping the two surfaces to the same orbifold $\mathcal{O}$, $\Phi : \mathbf{M}_1 \to \mathcal{O}$ and $\Psi : \mathbf{M}_2 \to \mathcal{O}$, taking corresponding landmarks to the same cone of $\mathcal{O}$, and defining the map via $f = \Psi^{-1} \circ \Phi$. A similar approach for disks was taken in [Weber and Zorin 2014; Aigerman et al. 2014]. A general approach for seamless surface mappings was recently discussed [Aigerman et al. 2015] however it is non-linear and can only guarantee reaching a local minimum of the functional, and is much more computationally expensive. Nevertheless, that method can handle an arbitrary number of landmarks.

We show six maps computed using this method in Figure 13, all of which are generated by four pairs of corresponding landmarks (depicted as colored spheres) using the type (iv) orbifold. The map is visualized by transferring a texture from the left surface to the right. Note that since we use boundaryless embeddings to a common orbifold to construct the final map, up to the choice of the homotopy class of the cut, it is not affected at all by the choice of cuts (*i.e.*, seamless). As exhibited in the mapping of the two busts, although we can set only four pairs of landmarks, the resulting map has good extrapolation properties in low curvature areas. It gracefully handles the mapping of the round sphere to the edged Tetrahedron, as well as mapping the Igea bust to the Tet. The conformal nature of the resulting map is also well suited to mapping highly non-isometric models such as the fish and bird. The mapping between the two humans exhibits the limitation of this method: Although it manages to produce a very natural map in almost all areas, using only four point constraints, the head is mapped incorrectly. Nonetheless, we believe the fact this method enables producing low distortion surface maps at the small price of solving two sparse linear systems will benefit algorithms which rely on searching exhaustively through low dimensional spaces of maps, such as RANSAC, or [Kim et al. 2011].

6.3 Other Euclidean orbifolds

Although the paper is focused on the spherical case, the orbifold-Tutte embedding can be used as-is for other Euclidean orbifolds. Figure 15 shows two parameterizations of a disk-type surface mesh to two different disk-type Euclidean orbifolds: a square and a right-angled isosceles triangle. In these cases, the orbifold is a topological disc with a boundary, and each side of the boundary of the orbifold is related to *itself* by a reflection in the group G. Therefore, in this case the transformations $R_{i'i}$ (with $i \equiv i'$) are reflections across each edge of the triangle, that is constraining the vertices to lie on the infinite line supporting the orbifold's edge.

Figure 14: *The orbifold-Tutte embedding can be used to create symmetric patterns on surface meshes. Left: The wallpaper group of the type (iv) orbifold enables seamlessly texturing the mesh with stripes. On the right, the wallpaper group of the type (ii) orbifold enables seamlessly texturing the mesh with equilateral triangles.*

The benefit in this embedding is that, in exception of the corners, all other boundary vertices are free to move and the map is still guaranteed to be bijective onto the target triangle or square.

We note that there are other disk-type Euclidean orbifolds that allow adding one or two cones *inside* the disk. The rest of the Euclidean orbifolds have the topology of the annulus, the Klein bottle, the Möbius strip, the real projective plane, and of course the torus [Conway et al. 2008]. All of these can be used as target domains for orbifold-Tutte embeddings. We strongly believe these will be useful for parameterization applications in the future.

Timings The algorithm was implemented in Matlab. The computations were performed on a 3.50GHz Intel i7 CPU. Typical times are: Parameterizing the lion-vase (39K vertices, 77K triangles) took 0.81 seconds, 0.59 of which spent on solving the linear system. Parameterizing the chinese dragon (655K vertices, 1.3M triangles) took 20 seconds, 19 of which were spent on solving the linear system.

7 Conclusions

We have presented a generalization of the convex-combination embedding to spheres. This results in seamless, globally injective parameterizations that approximate conformal mappings, and represent a bijection between the mesh and a Euclidean orbifold. The embedding is computed by solving a sparse linear system.

The main drawback of this approach is the limited family of cone structures that can be used. Basically, only cone structures for which a Euclidean orbifold exists are valid for the method; in case of a sphere, this gives four possible cone structures, with 3-4 cones.

Interesting future directions include generalizations to non-Euclidean orbifolds which allow more cones to be set. Another interesting research venue is using the 4-point maps for shape matching applications. Lastly, we note that we have no formal proof that the orbifold-Tutte embeddings converge to conformal maps (rather, only quite convincing empirical evidence) and while a proof is out-of-scope for this paper, we consider it important future work.

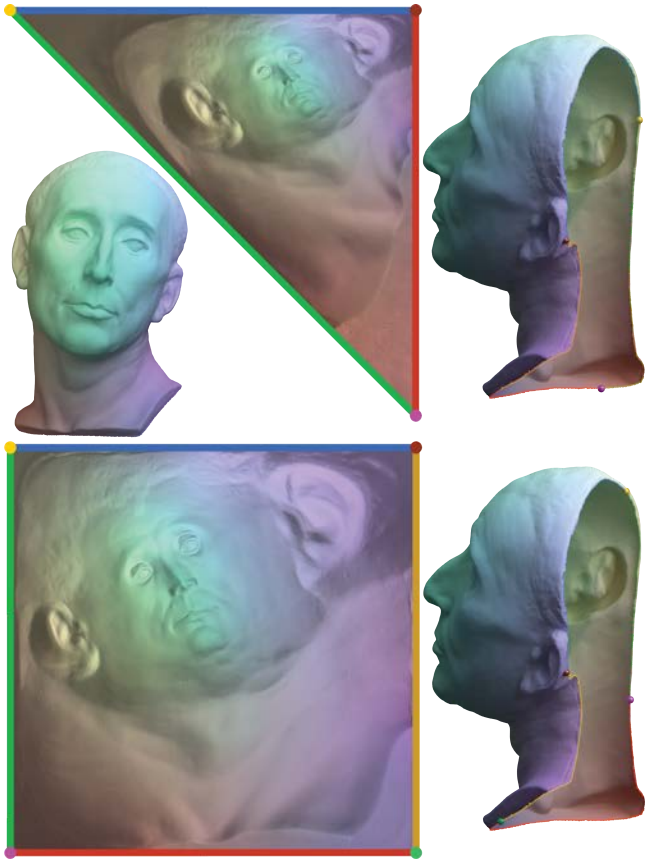

Figure 15: *Two orbifold-Tutte parameterizations of a disk-type surface to two different disk-type orbifolds: the square and the right-angled isosceles triangle. Although the boundary vertices are free to slide over the supporting line of their respective edge, the resulting embedding is guaranteed to be bijective.*

8 Acknowledgements

This work was funded by the European Research Council (ERC Starting Grant "SurfComp"), the Israel Science Foundation (grant No. 1284/12) and the I-CORE program of the Israel PBC and ISF (Grant No. 4/11). The authors would like to thank the anonymous reviewers for their comments and suggestions. The fish and bird models are from the SHREC07 dataset [Giorgi et al. 2007], the humans are from the SCAPE dataset [Anguelov et al. 2005], and all other meshes are from the aim@shape repository.

References

AIGERMAN, N., PORANNE, R., AND LIPMAN, Y. 2014. Lifted bijections for low distortion surface mappings. *ACM Transactions on Graphics (TOG) 33*, 4, 69.

AIGERMAN, N., PORANNE, R., AND LIPMAN, Y. 2015. Seamless surface mappings. *ACM Transactions on Graphics (TOG), in print*.

ANGUELOV, D., SRINIVASAN, P., KOLLER, D., THRUN, S., RODGERS, J., AND DAVIS, J. 2005. Scape: Shape completion and animation of people. *ACM Trans. Graph. 24*, 3 (July), 408–416.

BEN-CHEN, M., GOTSMAN, C., AND BUNIN, G. 2008. Conformal flattening by curvature prescription and metric scaling. In *Computer Graphics Forum*, vol. 27, Wiley Online Library, 449–458.

BOMMES, D., LÉVY, B., PIETRONI, N., PUPPO, E., SILVA, C., TARINI, M., AND ZORIN, D. 2013. Quad-mesh generation and processing: A survey. In *Computer Graphics Forum*, vol. 32, Wiley Online Library, 51–76.

BOMMES, D., LÉVY, B., PIETRONI, N., PUPPO, E., SILVA, C., TARINI, M., AND ZORIN, D. 2013. Quad-Mesh Generation and Processing: A Survey. *Computer Graphics Forum 32*, 6, 51–76.

CASTELLI ALEARDI, L., FUSY, R., AND KOSTRYGIN, A. 2014. Periodic planar straight-frame drawings with polynomial resolution. In *LATIN 2014: Theoretical Informatics*, A. Pardo and A. Viola, Eds., vol. 8392 of *Lecture Notes in Computer Science*. Springer Berlin Heidelberg, 168–179.

CONWAY, J. H., BURGIEL, H., AND GOODMAN-STRAUSS, C. 2008. The symmetries of things. *Appl Math Comput 10*, 12.

DESBRUN, M., MEYER, M., AND ALLIEZ, P. 2002. Intrinsic parameterizations of surface meshes. In *Computer Graphics Forum*, vol. 21, Wiley Online Library, 209–218.

FEINGOLD, D. G., AND VARGA, R. S. 1962. Block diagonally dominant matrices and generalizations of the gerschgorin circle theorem. *Pacific J. Math. 12*, 4, 1241–1250.

FLOATER, M. S., AND HORMANN, K. 2005. Surface parameterization: a tutorial and survey. In *Advances in multiresolution for geometric modelling*. Springer, 157–186.

FLOATER, M. 2003. One-to-one piecewise linear mappings over triangulations. *Mathematics of Computation 72*, 242, 685–696.

FLOATER, M. S. 2003. Mean value coordinates. *Computer aided geometric design 20*, 1, 19–27.

GIORGI, D., BIASOTTI, S., AND PARABOSCHI, L. 2007. SHREC: SHape REtrieval Contest: Watertight models track. *http://watertight.ge.imati.cnr.it/*.

GORTLER, S. J., GOTSMAN, C., AND THURSTON, D. 2006. Discrete one-forms on meshes and applications to 3d mesh parameterization. *Computer Aided Geometric Design 23*, 2, 83–112.

GOTSMAN, C., GU, X., AND SHEFFER, A. 2003. Fundamentals of spherical parameterization for 3d meshes. *ACM Transactions on Graphics (TOG) 22*, 3, 358–363.

GU, X., AND YAU, S.-T. 2003. Global conformal surface parameterization. In *Proceedings of the 2003 Eurographics/ACM SIGGRAPH symposium on Geometry processing*, Eurographics Association, 127–137.

HORMANN, K., AND GREINER, G. 2000. MIPS: An efficient global parametrization method. In *Curve and Surface Design: Saint-Malo 1999*, P.-J. Laurent, P. Sablonnière, and L. L. Schumaker, Eds., Innovations in Applied Mathematics. Vanderbilt University Press, Nashville, TN, 153–162.

KÄLBERER, F., NIESER, M., AND POLTHIER, K. 2007. Quadcover-surface parameterization using branched coverings. In *Computer Graphics Forum*, vol. 26, Wiley Online Library, 375–384.

KAZHDAN, M., SOLOMON, J., AND BEN-CHEN, M. 2012. Can mean-curvature flow be modified to be non-singular? *Comp. Graph. Forum 31*, 5 (Aug.), 1745–1754.

KHAREVYCH, L., SPRINGBORN, B., AND SCHRÖDER, P. 2006. Discrete conformal mappings via circle patterns. *ACM Transactions on Graphics (TOG) 25*, 2, 412–438.

KIM, V. G., LIPMAN, Y., AND FUNKHOUSER, T. 2011. Blended intrinsic maps. In *ACM Transactions on Graphics (TOG)*, vol. 30, ACM, 79.

KNÖPPEL, F., CRANE, K., PINKALL, U., AND SCHRÖDER, P. 2013. Globally optimal direction fields. *ACM Trans. Graph. 32*, 4.

KOBOUROV, S., AND LANDIS, M. 2007. Morphing planar graphs in spherical space. In *Graph Drawing*, M. Kaufmann and D. Wagner, Eds., vol. 4372 of *Lecture Notes in Computer Science*. Springer Berlin Heidelberg, 306–317.

LÉVY, B., PETITJEAN, S., RAY, N., AND MAILLOT, J. 2002. Least squares conformal maps for automatic texture atlas generation. In *ACM Transactions on Graphics (TOG)*, vol. 21, ACM, 362–371.

LOVÁSZ, L. 2004. Discrete analytic functions: an exposition. *Surveys in differential geometry 9*, 241–273.

MYLES, A., AND ZORIN, D. 2012. Global parametrization by incremental flattening. *ACM Transactions on Graphics (TOG) 31*, 4, 109.

MYLES, A., AND ZORIN, D. 2013. Controlled-distortion constrained global parametrization. *ACM Transactions on Graphics (TOG) 32*, 4, 105.

PALACIOS, J., AND ZHANG, E. 2007. Rotational symmetry field design on surfaces. In *ACM Transactions on Graphics (TOG)*, vol. 26, ACM, 55.

PINKALL, U., AND POLTHIER, K. 1993. Computing discrete minimal surfaces and their conjugates. *Experimental mathematics 2*, 1, 15–36.

RAY, N., LI, W. C., LÉVY, B., SHEFFER, A., AND ALLIEZ, P. 2006. Periodic global parameterization. *ACM Transactions on Graphics (TOG) 25*, 4, 1460–1485.

RAY, N., VALLET, B., LI, W.-C., AND LVY, B. 2008. N-symmetry direction field design. In *ACM Transactions on Graphics*. Presented at SIGGRAPH.

SCHWARTZ, R. E. 2011. *Mostly surfaces*, vol. 60. American Mathematical Soc.

SHEFFER, A., LÉVY, B., MOGILNITSKY, M., AND BOGOMYAKOV, A. 2005. Abf++: fast and robust angle based flattening. *ACM Transactions on Graphics (TOG) 24*, 2, 311–330.

SHEFFER, A., PRAUN, E., AND ROSE, K. 2006. Mesh parameterization methods and their applications. *Found. Trends. Comput. Graph. Vis. 2*, 2 (Jan.), 105–171.

SPRINGBORN, B., SCHRÖDER, P., AND PINKALL, U. 2008. Conformal equivalence of triangle meshes. *ACM Transactions on Graphics (TOG) 27*, 3, 77.

SUN, J., WU, T., GU, X., AND LUO, F. 2014. Discrete conformal deformation: Algorithm and experiments. *CoRR abs/1412.6892*.

TONG, Y., ALLIEZ, P., COHEN-STEINER, D., AND DESBRUN, M. 2006. Designing quadrangulations with discrete harmonic forms. In *Proceedings of the Fourth Eurographics Symposium on Geometry Processing*, Eurographics Association, Aire-la-Ville, Switzerland, Switzerland, SGP '06, 201–210.

TSUI, A., FENTON, D., VUONG, P., HASS, J., KOEHL, P., AMENTA, N., COEURJOLLY, D., DECARLI, C., AND CARMICHAEL, O. 2013. Globally optimal cortical surface matching with exact landmark correspondence. In *Proceedings of the 23rd International Conference on Information Processing in Medical Imaging*, Springer-Verlag, Berlin, Heidelberg, IPMI'13, 487–498.

TUTTE, W. T. 1963. How to draw a graph. *Proc. London Math. Soc 13*, 3, 743–768.

WEBER, O., AND ZORIN, D. 2014. Locally injective parametrization with arbitrary fixed boundaries. *ACM Transactions on Graphics (TOG) 33*, 4, 75.

Appendix A

Proof of Theorem 1. First, note that A is built out of 2×2 blocks

$$A = \begin{bmatrix} A_{11} & A_{12} & \cdots & A_{1n} \\ A_{21} & A_{22} & \cdots & A_{2n} \\ \vdots & \vdots & \ddots & \vdots \\ A_{n1} & A_{n2} & \cdots & A_{nn} \end{bmatrix}$$

where the blocks $A_{ij} \in \mathbb{R}^{2\times 2}$ are proportional to the identity matrix I, to a rotation $R_{i'i}$, or to the zero matrix 0. To show that A is non-singular we show that a different matrix A' with the same row span is non-singular. To build A', for each pair of twin boundary vertices (i, i') in $\mathbf{M}$ we use (9b) to cancel $\Phi_{i'}$ from (9a). This transforms equations (9a) to

$$\sum_{j\in\mathcal{N}_i} w_{ij}\,(\Phi_i - \Phi_j) + \sum_{j\in\mathcal{N}_{i'}} w_{i'j}\,\Phi_i - \sum_{j\in\mathcal{N}_{i'}} w_{i'j}\,R_{i'i}\Phi_j = c \quad (14)$$

where c stands for some constant defined according to the choice of $\Phi_j^{\mathcal{C}}$.

To show that A' is non-singular we will use a result by Feingold and Varga [1962] who generalized the theorem of non-singularity of diagonally dominant matrices to *block diagonally dominant*. A block matrix A is block diagonally dominant if for all i, A_{ii} is non-singular and

$$\left\|A_{ii}^{-1}\right\|^{-1} \geq \sum_{j\neq i} \|A_{ij}\| \quad (15)$$

where $\|\cdot\|$ can be taken as some arbitrary induced matrix norm. We choose $\|\cdot\|$ to be the matrix 2-norm, that is $\|A_{ij}\| = \sup_x \|A_{ij}x\|_2 / \|x\|_2$, where $\|\cdot\|_2$ is the standard Euclidean norm in $\mathbb{R}^2$. A block matrix A is *block-irreducible* if the $n \times n$ matrix with $\|A_{ij}\|$ in the $(i, j)^{\text{th}}$ entry is irreducible, that is represents a strongly connected directed graph. Feingold and Varga proved that an irreducible block diagonally dominant matrix with at least one strictly diagonally dominant block row (*i.e.*, strict inequality in (15) for some i) is non-singular.

We would like to apply this theorem to A'. Before doing that let us cancel all the variables Φ_k, $k = 1, .., J$ by substituting Eq. (8) into equations (7),(14). Now, all the block rows of A' corresponding to equations (7), (9b) and (14) are block diagonally dominant as defined in (15). The block rows of (7) and (14) for which there exist some $v_k \in \mathcal{C}$, $k = 1, .., J$ in the neighborhood of v_i or $v_{i'}$ are now strictly block diagonally dominant. Furthermore, A' is block irreducible as explained next. We need to show that the directed graph $\mathcal{G}$ corresponding to the matrix $(\|A_{ij}\|)_{ij}$ is strongly connected. The nodes of $\mathcal{G}$ are in one-to-one correspondence with the vertices of $\mathbf{M}$ excluding the cone vertices (*i.e.*, $\mathbf{V} \setminus \mathcal{C}$). Therefore, we will identify the nodes of $\mathcal{G}$ with the vertices of $\mathbf{M}$. Equations (7) imply that each node in the graph $\mathcal{G}$ corresponding to an internal vertex of $\mathbf{M}$ is connected to all its neighbors; equations (14) and (9b) imply that every node in $\mathcal{G}$ that corresponds to a boundary vertex in $\mathbf{M}$ is either connected to all its neighbors and the neighbors of its twin vertex, or connected just to its twin. Since $\mathbf{M}$ is connected (we assume here $\mathbf{M}$ remains connected after removing all the cone vertices), $\mathcal{G}$ is a strongly connected directed graph. Therefore, A' is irreducible and hence non-singular. This implies A is non-singular. □